Journal of Materials Chemistry C

ROYAL SOCIETY OF CHEMISTRY

PAPER

View Article Online
View Journal | View Issue

Cite this: J. Mater. Chem. C, 2024, 12, 5213

Magnetic properties of CrX_3 (X = Cl, Br, I) monolayers in excited states†

Prakash Mishra [a] and Tunna Baruah *[b]

Received 1st January 2024,
Accepted 6th March 2024

DOI: 10.1039/d4tc00003j

rsc.li/materials-c

The presence of intrinsic ferromagnetism in a new class of magnetic semiconductors CrX_3 (X = Cl, Br, I) in a reduced dimension is associated with magnetic anisotropy energy (MAE). MAE is relevant for the magnetic order of CrX_3. The control of magnetism in such 2D materials through external stimuli is gaining importance in view of potential technological applications. Here, we use all-electron density functional theory to investigate the magnetism of monolayers of chromium halides in excited states using a cluster model. We study the magnetization reversal barrier for two types of electronic singly excited states: (a) spin-preserving transitions, and (b) spin-flip transitions. While all the three halides show enhancement of MAE in excited states, the MAEs are significant for CrI_3 due to the large spin–orbit coupling in the iodines. The changes in the MAE in the excited state are influenced by the local charge distribution surrounding the iodine atoms. Using a model system, we also show that the MAE in chromium tri-iodides is strongly influenced by the charge transfer to the iodines in an excited state. Thus, controlling the charge transfer to the iodines can potentially be used to control the magnetization reversal barrier.

1 Introduction

The discovery of long-range magnetic order down to the monolayer in van der Waals layered crystals has led to intense research in the field of 2D magnetic materials.[1–8] Mermin and Wagner[9] had demonstrated that a 1- or 2-dimensional isotropic Heisenberg model with short-range exchange interaction prohibits long-range spin ordering at non-zero temperature. The magnetic ordering in the 2D materials such as monolayer CrI_3,[2] few-layer $Cr_2Ge_2Te_6$,[1] ferromagnetic monolayer VSe_2[10] and Fe_3GeTe_2[11,12] arises due to the magnetic anisotropy energy (MAE) that prevents spin fluctuation. The existence of magnetic properties in a reduced dimension has the potential to facilitate development of new advances in spintronics[13] and data storage devices.[3,4,14,15] The possibility of controlling the magnetism in such materials with external stimuli such as electric field,[5,16–19] photon,[20] doping,[21–23] intercalation[24] and strain[25–29] opens up the field for further advances.

In the present work, we focus on the series of semiconductors CrX_3 (X = Cl, Br, or I)[30–33] that exhibit a range of intriguing properties, including ferromagnetism in monolayers, magneto-optical Kerr[1,2] and Faraday effects,[34] large tunnel magneto-resistance effects,[35–38] and polarized photoluminescence.[39] In chromium trihalides, the Cr^{3+} ions are octahedrally coordinated with halides. The edge-sharing octahedral units form a honeycomb net. Using a combination of tunneling and magneto-optical measurements on few-layer and bi-layer samples of CrX_3, Kim *et al.* established the ferromagnetic nature of monolayers of $CrBr_3$ and CrI_3.[40] Although the chromium halides have similar structures, the magnetic interaction is different. The interlayer interaction in bromide and iodide is ferromagnetic[32,41,42] whereas in chloride it is antiferromagnetic.[43,44] On the other hand, both bromide and iodide have an out-of-plane easy axis,[45] and the chloride has an easy plane of magnetic anisotropy.[46,47]

The dependence of magnetism in these systems on physical stimuli such as pressure,[48–50] temperature,[51] and, electric field[5,16–19] has displayed a rich phenomenon. Singamaneni *et al.*[52] have shown that the magnetic properties of the $CrCl_3$ and CrI_3 crystals show an enhancement in the saturation magnetization which is explained through ligand to metal charge transfer that results in a mixture of Cr^{3+} and Cr^{2+} ions in the crystal.[53] In recent years, various computational methodologies such as density functional theory (DFT), quantum Monte Carlo, and machine learning models have been used to determine the magnetic properties such as inter and intra-layer exchange coupling and magnetic anisotropy of these systems.[54–57] Scientists have been exploring the optical manipulation to tune and enhance light-modulated magnetism. Laser

[a] Computational Science Program, University of Texas at El Paso, El Paso, Texas 79968, USA
[b] Department of Physics, University of Texas at El Paso, El Paso, Texas 79968, USA. E-mail: tbaruah@utep.edu

† Electronic supplementary information (ESI) available. See DOI: https://doi.org/10.1039/d4tc00003j

excitation can induce ultrafast (femtosecond) charge transfer from X to Cr, and magnetic properties can be enhanced. This enhancement is reported to last for a relatively long time. Liu *et al.* used the density functional theory and real-time time-dependent density functional (rt-TDDFT) methods for the optical manipulation of magnetic properties in monolayer CrX_3.[58,59] Yang *et al.* reported nonmetallic atom-induced MAE in monolayer $CrBr_3$ and CrI_3.[60] In this work, we systematically investigate the electronic structure and magnetic properties of the monolayer chromium trihalides in electronic excited states using DFT. Since the MAE is relevant for the magnetic order in 2D materials, our goal is to examine how the MAE changes in electronic excited states. The electron density changes in the excited states result in changes in the spin–orbit coupling strengths. We examine the MAE for singly excited particle–hole states in this work. We show that the MAE is enhanced for several excited states of the monolayer chromium trihalides for both spin-conserving and spin-flip excited states.

In the next section, we describe the methods used in these calculations and other computational details. The results of the three monolayer chromium trihalides are presented and discussed in Section III.

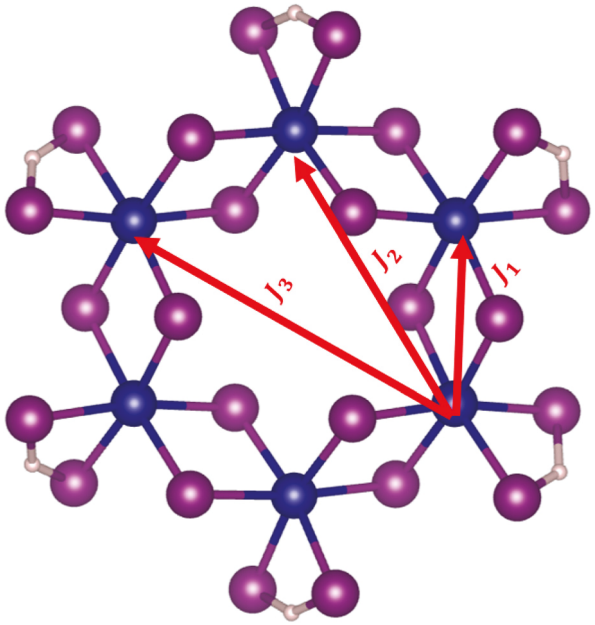

Fig. 1 The optimized structure of CrX_3 (X = I, Br, Cl) calculated using the PBE functional with the color scheme blue = Cr, purple = X, and white = hydrogen.

2 Computational details

For the calculations presented here, we use a cluster model for the monolayer chromium trihalides. This choice is based on access to the source code and enhanced features in the molecular code that the authors have used and developed in past.[61–63] The cluster model for the monolayer chromium trihalides has a hexagonal motif with six Cr ions each of which is octahedrally coordinated with six halides as shown in Fig. 1. The Cr atoms in these compounds are in an oxidation state of +3 and an electronic configuration of [Ar] $4s^0$ $3d^3$, which results in a spin $S = 3/2$ per Cr atom. To maintain the similarity to the bulk structures and the charge state of the Cr ions, we have passivated the halides with H atoms. The H atoms are chosen such that the magnetic moment of the cluster is $18\mu_B$ or $3\mu_B$/Cr. The resulting six-center clusters have six-fold symmetry.

All the calculations reported here are carried out using the NRLMOL code.[61–63] This code uses a Gaussian basis set and the calculations are done at the all-electron level using the generalized gradient approximation (GGA) of the Perdew–Burke–Ernzerhof functional[64,65] and the NRLMOL default basis set.[63] The bond lengths of the optimized lowest energy configurations shown in Table 1 are in good agreement with those reported in the literature for monolayer chromium trihalides.

We utilized the perturbative delta-SCF method[66,67] to determine the total energies and single particle orbitals and eigenvalues for the excited states. This method accounts for a single excitation from an occupied state to a virtual state. This variant of the standard delta-SCF approach imposes an orthogonality constraint between the ground state and excited state single determinantal wave functions by relaxing the occupied orbitals in the unoccupied orbital space and the hole orbital in the occupied orbital space. The excited state energies are determined from the total energy difference between the ground and the excited states. Details of this method can be found in ref. 66 and 67.

Table 1 Structural parameters of the CrX_3 cluster relaxed with PBE functional

	Cr–X (Å)		Cr–Cr (Å)	
Compound	Calc.	Expt.[a]	Calc.	Ref. 7
$CrCl_3$	2.38	2.36	3.52	3.49
$CrBr_3$	2.52	2.52	3.72	3.72
CrI_3	2.74	2.80	4.04	4.026

[a] Ref. 33.

The dipole transition matrix elements determine the probability of dipolar transitions. These are calculated from the particle and hole orbitals using $d_{ph} = \left\langle \psi_h | \vec{\mu} | \psi_p \right\rangle$, where μ is the dipole operator.

The MAE was determined using the approach outlined in ref. 68. In this approach, the spin–orbit coupling is calculated using the second-order perturbation method. For the excited states, the occupied orbitals and their energies from the perturbative delta-SCF approach are used as the reference state to calculate the MAE. While the excited states are obtained only for a single particle–hole excitation, this approximate method can still show the trends for different halides.

3 Results and discussion

3.1 Ground states

To validate the cluster model, we present the atom-projected density of states (DOS) for the three monolayer chromium

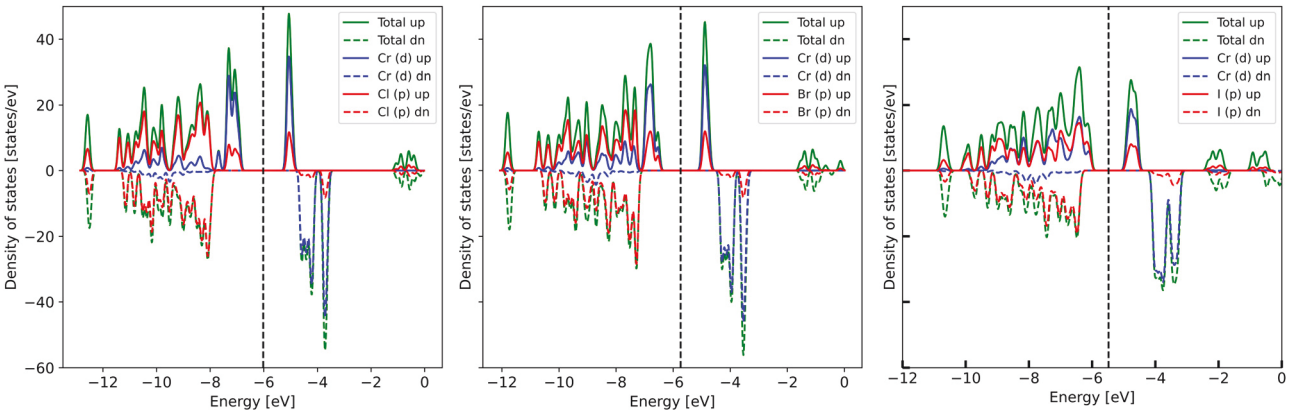

Fig. 2 Total and projected density of states on the Cr-d and halide p states for CrX_3 with (a) X = Cl, (b) X = Br, and (c) X = I.

trihalide compounds in Fig. 2. The DOS shows the contribution from the Cr-d states and the halide-p states for the frontier orbitals in the majority spin channels. These plots are in good agreement with earlier DFT calculations with the PBE functional from ref. 69 using periodic boundary conditions. Our calculated energy gaps between the highest occupied molecular orbital (HOMO) and the lowest unoccupied molecular orbitals (LUMOs) in the three systems are 1.77, 1.56, and 1.17 eV in good agreement with the values of 1.52, 1.33, and 1.14 eV reported by Zhang *et al.*[69] using the pseudopotential and PBE functional for the monolayer chromium trihalides. The gap is larger in our calculations due to the quantum confinement effects. These plots also show that the HOMO–LUMO gap is in the majority spin channel with the minority spin gap being very large.

To further validate the structures, Heisenberg exchange coupling constants were also determined using the broken symmetry approach.[70] We use a four-state energy mapping methodology, as described in ref. 69. The total energy can be written as

$$E = E_0 - \sum_{i,j} J_1 S_i \cdot S_j - \sum_{i,j} J_2 S_i \cdot S_j - \sum_{i,j} J_3 S_i \cdot S_j, \qquad (1)$$

where J_1, J_2, and J_3 are the first, second, and third nearest neighbor exchange coupling parameters and E_0 is energy without the exchange interactions. In our cluster model, this amounts to taking into account six first and second-nearest neighbors, and three third-nearest neighbor interactions as shown in Fig. 1. To prevent the relaxation of magnetic moments into the ground-state configuration or any stable configuration other than the desired one during the self-consistent procedure, the magnetic moments were constrained to the desired directions for different magnetic configurations. The calculated exchange coupling parameters J_1, J_2, J_3 presented in Table 2 are in good agreement with the previous studies for the three CrX_3 trihalides.[69] The first nearest-neighbor interaction is the most dominant one in these systems. The differences with the earlier calculations are on the order of 10^{-4} eV which can arise not only from the low dimension of the structure but also from the use of pseudopotentials in the periodic calculations. For CrI_3, the J_3 parameter has the opposite sign indicating an antiferromagnetic alignment. However, since the nearest neighbor coupling is the most dominant one with an order of magnitude larger values, this discrepancy can be neglected. Moreover, such a discrepancy is also seen between previously reported values, *e.g.* ref. 71. Overall, we find that the cluster model can well represent the monolayer chromium trihalides for the purposes of this work.

Table 2 Exchange coupling parameters for CrX_3 in meV. The earlier calculated values for monolayers from ref. 69 are shown in parentheses

Compound	J_1 (meV)	J_2 (meV)	J_3 (meV)
$CrCl_3$	1.47 (1.92)	0.21 (0.23)	−0.13 (−0.13)
$CrBr_3$	2.2 (2.60)	0.33 (0.38)	−0.11 (−0.15)
CrI_3	2.77 (2.86)	0.74 (0.64)	0.15 (−0.15)

Our calculated MAE values of $CrCl_3$, $CrBr_3$, and CrI_3 in the ground state are 1.58, 14.51, and 68.47 K, respectively which on a per Cr basis are 0.26, 2.41, and 11.41 K. These values are in good agreement with the previously calculated values for the three monolayer CrX_3 trihalides[69] of 0.36 K, 2.15 K, and 7.95 K per Cr in these materials with the PBE functional and pseudopotential. We point out that the GGA+U method results in anisotropy per Cr values that range from 0.29–0.35 K for chloride, 1.74–1.85 K for bromide, and 8.58–9.33 K for the iodide compounds.[47,72] In the cluster model used in this work, the ratio of the halides to the Cr atom is larger compared to the monolayer which is likely the reason for the larger per Cr MAE values, particularly for the iodide. Since the charge state of the Cr ions is the same in all three halides, the large change in magnetic anisotropy energy arises from the spin–orbit coupling in the halides of the system. CrI_3 has the highest anisotropy energy due to the large spin–orbit interaction in the iodine atoms. Using the atom-centered Gaussian basis sets, it is possible to decompose the anisotropy Hamiltonian into a sum of atom-centered terms. This scheme allows one to project the MAE into individual atoms in the system.[73] This scheme assumes that single-center diagonal terms of the anisotropy Hamiltonian is most dominant. The atom projected MAE (PMAE) shows the orientation of the local easy, medium, and

hard axes on the atoms. Since CrI_3 has the largest MAE, we discuss this system in more detail below.

In the CrI_3 cluster, there are two different types of coordination for the I atoms as can be seen from Fig. 3, and accordingly the PMAE value varies for each type of iodine atom. Each Cr is octahedrally connected with six iodines. Two such iodines between two octahedra form bonds with two Cr ions. These are the iodines in the bridge positions The PMAE of the iodines in the bridge positions is higher compared to the terminal iodines that are passivated with hydrogen and connected to a single Cr ion. The octahedrons are rotated to form the ring shown in Fig. 3. The PMAE for the bridging iodines is larger with an average value of $\sim$21.37 K whereas the terminal iodines coordinated with hydrogens have a site average of $\sim$4 K, respectively. The iodines have non-zero spin moments with the largest moments on the order of $0.1\mu_B$ on the bridge iodines. The passivation with the hydrogens reduces the average local moments to $0.035e$ on the terminal iodines and also with smaller PMAE. The PMAE on the Cr atoms is much smaller on the order of $\sim$0.36 K although the spin moments on the Cr atoms are on the order of $2.98\mu_B$. The large MAE contributions from iodine atoms have also been reported by Yang *et al.*[60] The global easy axis of magnetization is out-of-plane which is the *z*-axis in Fig. 3. The orientations of the local easy axes on the iodines in the bridge positions are shown in Fig. 3. Although the local easy axes are not aligned along the global easy axes, the easy axes on all atoms combine to produce the global out-of-plane easy axis. The symmetry of the cluster is not strictly enforced during geometry optimization, as a result, there is slight symmetry breaking which results in differences in the orientation of the magnetization axes. Overall, the local easy axis orientations in the ground state reflect the symmetry of the system.

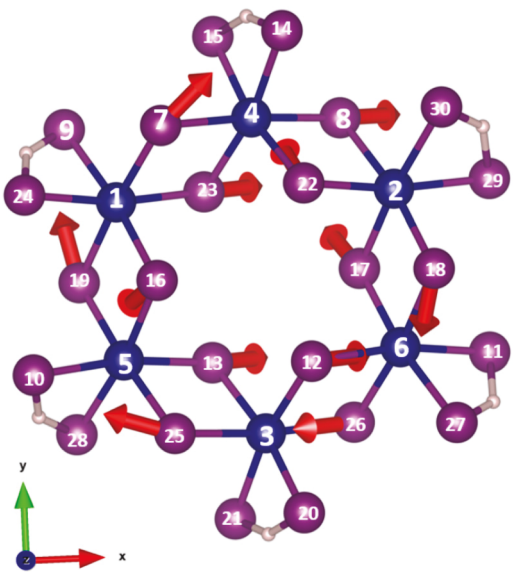

Fig. 3 Schematic representation of CrI_3 with atom index for each atom and the local easy axis directions on the bridging iodine atoms for the ground state of CrI_3.

On the other two complexes, the local PMAEs on the halides are much smaller leading to smaller total anisotropy energies. PMAE patterns resemble those of the CrI_3 cluster but with significant reductions for bromine and chlorine atoms. The bridging bromine atoms have an average PMAE of $\sim$2.75 K, whereas this value for similarly situated chlorine atoms is $\sim$0.11 K. The halides in the terminal positions coordinated with hydrogens show much smaller PMAEs of 0.95 K for Br and 0.05 K for chlorines. In these two compounds, the Cr atoms have PMAE values around $\sim$0.17 K and $\sim$0.13 K, closely resembling those of CrI_3. Overall, bromine and chlorine atoms contribute significantly less to PMAE compared to iodine atoms which shows that the spin–orbit coupling in the halides plays a significant role in determining the magnetic properties of these compounds (Table 3).

3.2 Excited states

The DOS shown in Fig. 2 shows that the frontier orbitals belong to the majority spin and the HOMO–LUMO gap in the majority spin channel is much smaller compared to that of the minority spin in all three compounds. Therefore, we considered only the majority spin singly excited states. These excited states are calculated using the perturbative delta-SCF method which orthogonalizes the excited state Slater determinant to the ground state one and the energies of the excited states are determined from the total energy differences. In this work, we considered two types of transitions, spin-preserving and spin-flip transitions. We considered particle–hole excited states from 12 occupied frontier orbitals that form a band near the Fermi level to the twelve lowest unoccupied ones which form the lowest band of unoccupied orbitals in the DOS plot. These orbitals have a large Cr d-character. This choice of particle and hole states also depends on the excitation energies. The calculations were restricted to excited states roughly within 4 eV above the ground state. For each singly excited state, the MAE and the spin moments on the Cr ions are also calculated. The ground state dipole moments in our model are 0.26, 0.15, and 0.62 Debye for the $CrCl_3$, $CrBr_3$, and CrI_3 systems. The small values of dipole moments show the isotropy of the charge distribution in the clusters in the ground state. We also calculated the dipole moments in the excited states to identify the charge transfer states. Since the numbers of particle–hole states calculated for each halide are large we present the data as ESI.† The excitation energies, MAEs, dipole moments in the excited states, transition dipole matrix elements ($|d_{ph}|^2$), and population analysis for the singly excited spin conserving excited states of the CrI_3, $CrBr_3$, and $CrCl_3$ are presented in Tables S1–S3 (ESI). In the tables, the occupied and unoccupied

Table 3 The site average PMAE values in Kelvin for the halides and Cr atoms in CrX_3

Compound	Bridge (K)	Terminal (K)	Cr (K)
$CrCl_3$	0.11	0.05	0.13
$CrBr_3$	2.75	0.95	0.17
CrI_3	21.37	4.59	0.36

states are labeled according to their position with respect to the HOMO and LUMO. Thus H-n refers to nth orbital below the HOMO and L+m refers to the mth orbital above the LUMO. The perturbative delta-SCF energies take into account the particle–hole interaction. In DFT, the virtual orbitals do not hold the same meaning as in Hartree–Fock. Therefore, for a given hole state, the transition energies do not necessarily increase relative to the previous transition. The lowest excitation energies are 1.88, 1.62, and 1.34 eV for $CrCl_3$, $CrBr_3$, and CrI_3, respectively. These energies are slightly higher than the respective HOMO–LUMO gaps.

The same calculations were also carried out for spin-flip excitations for single particle–hole states. Since the frontier orbitals are of majority spin, the spin-flip excitations involve the majority to minority spin transitions. Thus, such excitations lead to a lowering of the total spin moment on the cluster to $16\mu_B$. The spin flip transitions in general have a higher threshold energy in all the three systems. The excited state energies, MAE, dipole moments, and average spin moments on Cr for the spin-flip excitations of the CrI_3, $CrBr_3$, and $CrCl_3$ are provided in S4, S5, and S6 for the three halide systems.

The MAE values in various excited states for the three different chromium trihalide clusters are shown in Fig. 4 which shows the MAE values for both the spin-conserving and spin-flip transitions. These plots are restricted to 3 eV above the ground state. In these figures, the dashed line represents the ground state MAE. For $CrCl_3$, although all transitions tend to increase the MAE, the overall strength of the MAE is still quite small for both the spin-conserving and spin-flip transitions. The largest MAE value for the spin-conserving transitions in this system is less than 12 K, whereas for spin-flip transitions it is slightly higher. The largest MAE value rises to 22 K for $CrBr_3$ for excitation energies within 3 eV considering both the spin conserving and spin-flip transitions. Compared to the ground state MAE, the largest excited state MAE shows a 51% increase for $CrBr_3$ but by 500% change for $CrCl_3$. The CrI_3 system is the strongest magnet among the three systems. The large spin–orbit coupling of CrI_3 leads to large MAE values for the ground state compared to the other two halides. The MAE value for CrI_3 in the ground state is 68.47 K which translates to 11.4 K per Cr. For the spin-conserving excited states within 3 eV, the largest value of MAE is $\sim$158.2 K which is more than double of the ground state value. The dipole transition matrix element values increase from the chloride to the iodide which likely results from more hybridization between Cr d and halogen p states for the larger halogen atoms. For spin-flip transitions too we find that there are a few outlier states with similar large MAEs.

To understand the origin of the large anisotropy energies of CrI_3 in the excited states, we considered in detail the changes in the local anisotropy energy for a few of the excited states. The PMAE values on the Cr and the bridging and a few of the terminal iodines are listed for several excited states and the ground state in Table 4. The sites 1–6 correspond to the Cr atoms in this table. One of the excited states considered here is H $\rightarrow$ L+7 transition. Assuming small changes in the passive orbitals, the difference between the particle and hole density shows the change in the total electron density upon electronic excitation. This density difference between the particle and the hole orbitals for the H $\rightarrow$ L+7 state is shown in Fig. 5. From the DOS plot (Fig. 2), it can be seen that the HOMO of CrI_3 has a

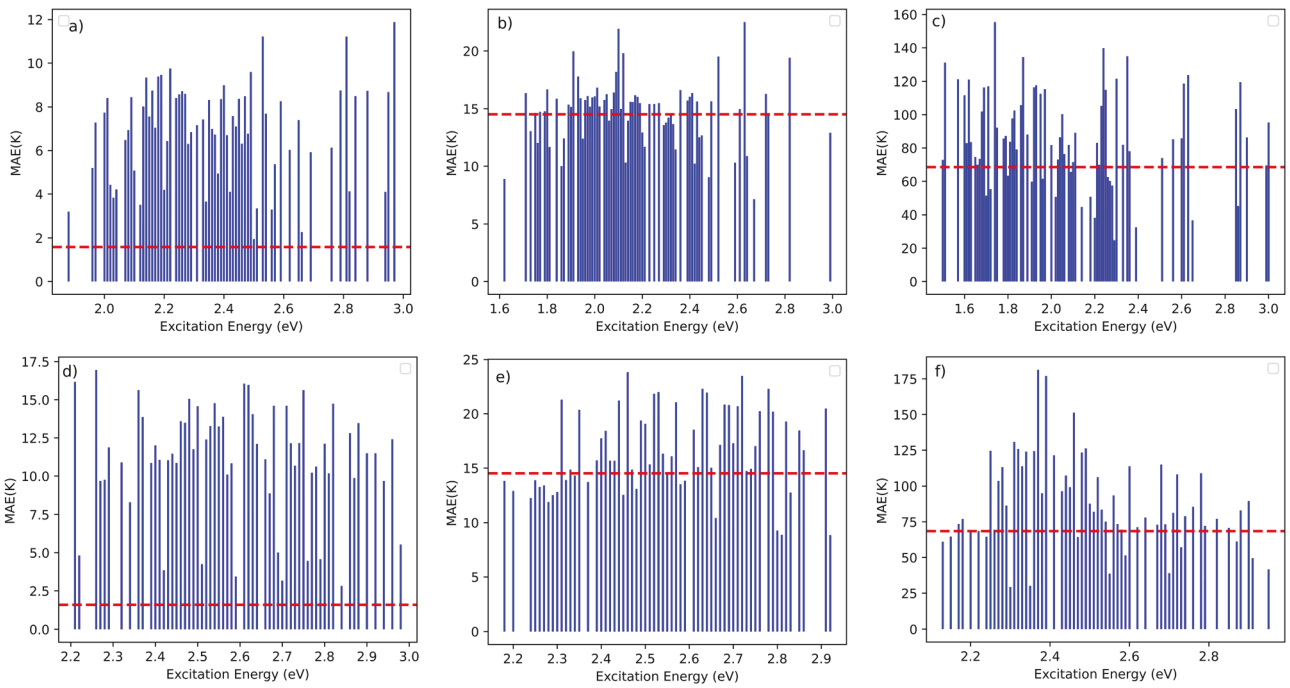

Fig. 4 MAE (K) as a function of excitation energy (eV) for spin-conserving single particle–hole transitions of CrX_3 for X = (a) Cl, (b) Br, (c) I and spin-flip transitions for X = (d) Cl, (e) Br, and (f) I. The dashed line represents the ground state MAE.

Table 4 Projected magnetic anisotropy energies (PMAEs) on the Cr, bridge (Br), and a few terminal (Tr) iodine sites for CrI_3 in singly excited particle–hole states. The ground state (GS) PMAEs are also included for reference

		Spin preserving		Spin flip	
Atom	Site	H → L+9	H → L+7	H−2 → L+9	GS
Cr	1	2.46	0.32	2.56	0.31
	2	0.29	1.14	4.61	0.28
	3	0.74	2.09	3.72	0.43
	4	0.39	0.41	2.28	0.48
	5	8.42	9.34	2.01	0.37
	6	0.50	0.59	2.50	0.30
I (Br)	7	19.64	13.55	16.35	17.90
	8	20.48	19.39	20.18	18.21
	12	16.10	24.35	17.42	22.09
	13	18.23	6.53	19.93	23.08
	16	25.66	75.90	16.02	25.09
	17	32.77	34.69	12.15	30.61
	18	18.49	19.47	18.85	17.93
	19	20.62	42.64	17.14	16.17
	22	19.31	25.65	22.40	21.59
	23	27.91	11.23	17.62	27.82
	25	18.19	39.54	17.91	17.51
	26	18.37	29.07	19.28	18.60
I (Tt)	28	3.36	6.11	4.58	3.85
	10	4.75	5.15	6.31	4.91
	24	1.99	5.55	6.82	5.59
	9	3.58	1.82	4.85	3.52

similar amount of iodine-p and Cr-d character, whereas the unoccupied orbitals have more Cr-d character. This transition increases the spin charge on Cr_5 which also shows a large increase of PMAE to 9.34 K. However, the large change in the total anisotropy energy arises from changes in charge density on the iodines. The PMAE on the iodines shows a large change for several of the iodine atoms. While the PMAE on one of the iodines increases to 75.9 K, a decrease in PMAE for another iodine to nearly 6.53 K is also seen. The PMAE values for terminal iodines do not show significant change. The global easy axis for this state lies along the *z*-axis which is the out-of-plane direction.

The spin-flip transitions on the CrI_3 show that the site average spin moment on the Cr atoms is lower compared to the ground state but the spin moments on the iodines are larger. The spin-flip transition H−2 → L+9 state results in a large MAE. In this case, we find that the PMAEs on iodines are lower but the PMAEs on Cr are relatively larger than those in the ground state. This state also has a global easy axis of magnetization that points out of the plane of the cluster.

Next, we considered the spin conserving H → L+9 state which has a much lower MAE of 36.71 K compared to the ground state (Fig. 6). The PMAE on the Cr shows a similar trend to H → L+7 but the PMAEs on the iodines are on the same order of magnitude as for the ground state. However, we find that the global easy axis of the H → L+7 state is out-of-plane, whereas for the H → L+9 state, it is in a general direction not aligned with the cluster symmetry. Examination of a few other states however showed that the out-of-plane direction of the global easy axis is not always associated with a large value of MAE. For several excited states, we find that the MAE is large although the global easy axis is in a general direction. The local environment around the iodines determines the PMAE and the local easy axis direction. However, alignment or non-alignment of the local axes can influence the barrier.

Qualitatively, in the CrX_3 systems, the Cr ions are in the +3 charge state and a charge transfer from the Cr to the halides

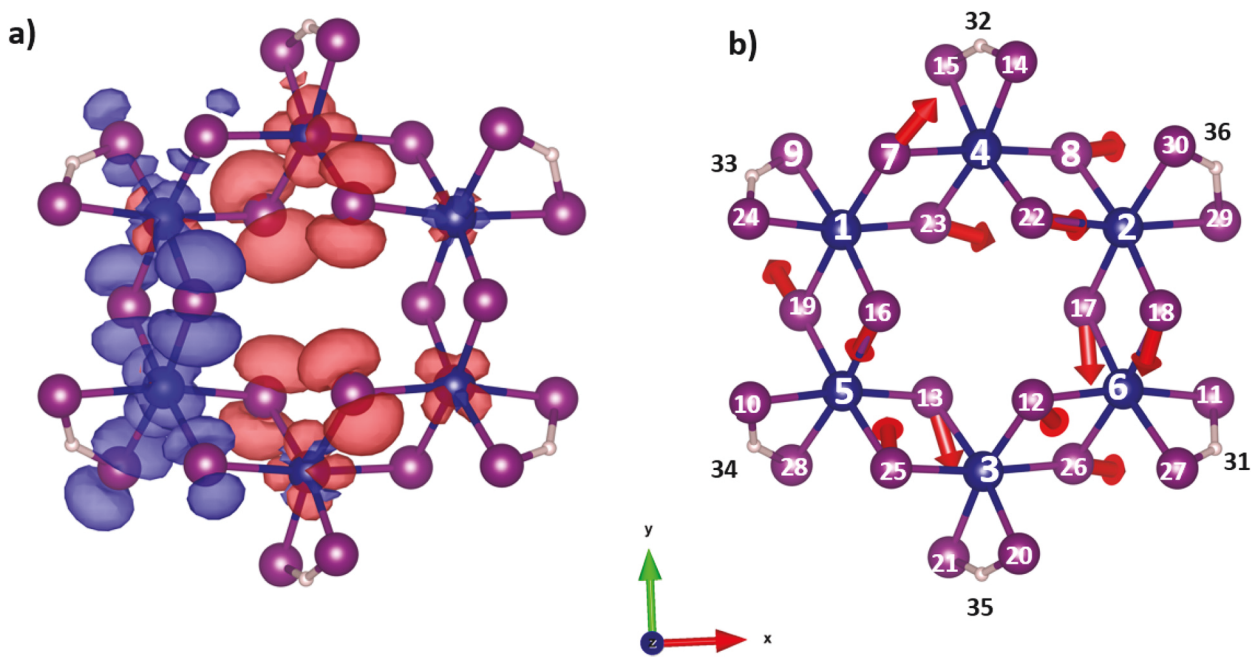

Fig. 5 (a) Orbital densities of H → L+7 transition of CrI_3. All isosurface values are 0.0001 a.u. Blue and red surfaces correspond to the L+7 and the H orbitals, respectively. (b) Local easy axes on bridge iodines are shown for the H → L+7 transition.

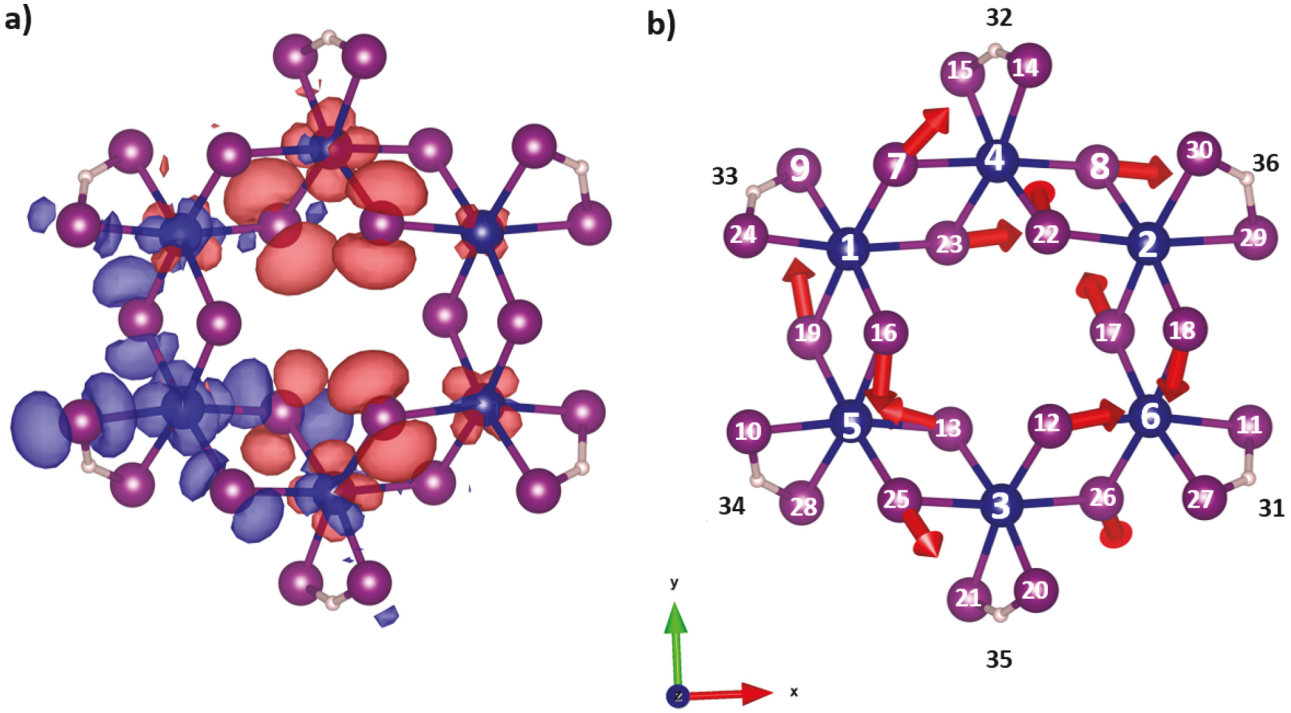

Fig. 6 (a) Orbital densities of the H → L+9 transition of CrI_3. All isosurface values are 0.0001 a.u. Blue and red isosurfaces correspond to the L+9 and the H orbitals, respectively. (b) Easy axis directions on the bridging iodines in the H → L+9 state.

takes place in the ground state leading to the formal charge of −1 on the iodines. However, the presence of small spin charges on the iodines indicates that the charge transfer is not complete and the iodines are not in the −1 anionic state. When charge transfer from Cr to I is complete, iodines are in a close shell structure with very little contribution to the MAE. On the other hand, large contributions may arise when the charge transfer is incomplete such that the iodine has a slightly open p-shell. Spin charge on the iodines may also occur in the situation where the iodines have more than 1 extra electron. In that case, however, the extra charge will occupy the next s-orbital with a locally spherically symmetric charge distribution. As a result, the MAE for such iodine will be small although there is a small spin moment on that ion. To check this hypothesis, we carried out additional calculations on a charged CrI_3 4-atom model system which has the same stoichiometry as the monolayer. The spin on the molecule was allowed to change from the $S = 3/2$ in the neutral state. The charge was increased from +1 to −1 in steps of $0.2e$. The corresponding spin-charge on the Cr and iodines, MAE, and PMAE on the Cr and iodines are shown in Table 5. In the neutral state, the iodines already have a small spin charge on them less than $0.1\mu_B$. In this state the total magnetic moment of the molecule is $3\mu_B$. When a small fractional charge is removed from the molecule, the total magnetic moment decreases with a similar change in the magnetic moment on the Cr. Similarly, the addition of a small electron charge results in a larger spin charge on the Cr and a larger total spin moment for the molecule. Removal of fractional charges from the molecule results in the increase of spin charges on the iodines and the total MAE of the molecule with a commensurate increase of PMAE on the iodines. On the other hand, as the extra fractional electronic charge is added, the total MAE decreases and the PMAE on the iodines also becomes small. The large PMAE on the iodines in the cluster therefore arises due to small fractional charges on the iodines that likely result from incomplete charge transfer from the Cr to the iodines. The excited states involve charge transfer from one region to another of the cluster which in turn leads to large or small PMAE on iodines depending on the saturation of the p-shell.

Table 5 Calculated magnetic moment (μ_B), MAE (K), and PMAE (K) of the CrI_3 model system in different charge states

	Magnetic moment (μ_B)			PMAE (K)	
Charge	Cr	I	MAE (K)	Cr	I
1	2.65	−0.22	159.14	3.93	38.78
0.8	2.7	−0.19	141.35	3.06	47.86
0.6	2.76	−0.16	138.42	2.69	87.84
0.4	2.83	−0.14	109.73	2.84	53.08
0.2	2.9	−0.11	102.44	2.02	50.98
0	2.98	−0.09	37.28	3.78	6.26
−0.2	3.1	−0.08	20.56	3.16	4.75
−0.4	3.16	−0.06	12.27	2.58	2.95
−0.6	3.25	−0.04	20.88	2.67	2.67
−0.8	3.34	−0.03	19.62	2.26	1.97
−1	3.43	−0.01	4.62	1.57	1.57

4 Conclusions

We carried out DFT calculations on a cluster model of a monolayer of CrX_3 to investigate the MAE in spin-conserving and spin-flip single particle–hole excited states. Employing the

perturbative delta-SCF method, we determined that the MAE exhibits notable variations depending on the specific electronic transitions considered. Among the three halides, the MAE is significant for the iodide system due to the strong spin–orbit coupling in the iodines. The projected anisotropy energies on the iodines are larger than on the Cr ions although the spin moments on the Cr ions are order of magnitude larger than those on the iodines. Using a toy model system, we show that the charge transfer to the iodines strongly influences the MAE of the cluster. The charge transfer from the Cr to the halides is not complete with some back transfer from the ligand to the metal. The incomplete p-shell closure results in large MAE for iodine-based systems. Due to the excitations, there can be large variations in the PMAE of iodines in a given excited state. Moreover, the global easy axis shows variations in the excited states. The global easy axis of a cluster is determined by the local easy axes. We also find that the local anisotropy axes on the halides follow the symmetry of the cluster in the ground state with an out-of-plane global easy axis. In most of the excited states, the global easy axis is in the out-of-plane direction but there are also cases where the global easy axis lies in a general direction. Overall, in both the ground and excited states the magnetic properties are dependent on the non-magnetic halide atoms.

Conflicts of interest

There are no conflicts to declare.

Acknowledgements

The authors acknowledge computational help from Dr Y. Yamamoto and Dr Po-Hao Chang and discussions with Profs. M. Pederson and S. Singamaneni. This work was supported by the National Science Foundation (NSF-DMR) under Award No. 2105109. TB gratefully acknowledges partial support from the US Department of Energy, Office of Science, Office of Basic Energy Sciences, as part of the Computational Chemical Sciences Program under Award No. DE-SC0018331. Support for computational time at the Texas Advanced Computing Center and NERSC is gratefully acknowledged.

Notes and references

1 C. Gong, L. Li, Z. Li, H. Ji, A. Stern, Y. Xia, T. Cao, W. Bao, C. Wang and Y. Wang, *et al.*, *Nature*, 2017, **546**, 265–269.
2 B. Huang, G. Clark, E. Navarro-Moratalla, D. R. Klein, R. Cheng, K. L. Seyler, D. Zhong, E. Schmidgall, M. A. McGuire and D. H. Cobden, *et al.*, *Nature*, 2017, **546**, 270–273.
3 K. S. Burch, D. Mandrus and J.-G. Park, *Nature*, 2018, **563**, 47–52.
4 C. Gong and X. Zhang, *Science*, 2019, **363**, eaav4450.
5 K. F. Mak, J. Shan and D. C. Ralph, *Nat. Rev. Phys.*, 2019, **1**, 646–661.
6 B. Huang, M. A. McGuire, A. F. May, D. Xiao, P. Jarillo-Herrero and X. Xu, *Nat. Mater.*, 2020, **19**, 1276–1289.
7 D. Soriano, M. I. Katsnelson and J. Fernández-Rossier, *Nano Lett.*, 2020, **20**, 6225–6234.
8 J. Kim, K.-W. Kim, B. Kim, C.-J. Kang, D. Shin, S.-H. Lee, B.-C. Min and N. Park, *Nano Lett.*, 2019, **20**, 929–935.
9 N. D. Mermin and H. Wagner, *Phys. Rev. Lett.*, 1966, **17**, 1133–1136.
10 M. Bonilla, S. Kolekar, Y. Ma, H. C. Diaz, V. Kalappattil, R. Das, T. Eggers, H. R. Gutierrez, M.-H. Phan and M. Batzill, *Nat. Nanotechnol.*, 2018, **13**, 289–293.
11 Z. Fei, B. Huang, P. Malinowski, W. Wang, T. Song, J. Sanchez, W. Yao, D. Xiao, X. Zhu and A. F. May, *et al.*, *Nat. Mater.*, 2018, **17**, 778–782.
12 Y. Deng, Y. Yu, Y. Song, J. Zhang, N. Z. Wang, Z. Sun, Y. Yi, Y. Z. Wu, S. Wu and J. Zhu, *et al.*, *Nature*, 2018, **563**, 94–99.
13 I. Žutić, J. Fabian and S. D. Sarma, *Rev. Mod. Phys.*, 2004, **76**, 323.
14 Z. Jiang, P. Wang, J. Xing, X. Jiang and J. Zhao, *ACS Appl. Mater. Interfaces*, 2018, **10**, 39032–39039.
15 Z. Liu, J. Liu and J. Zhao, *Nano Res.*, 2017, **10**, 1972–1979.
16 S. Jiang, J. Shan and K. F. Mak, *Nat. Mater.*, 2018, **17**, 406–410.
17 B. Huang, G. Clark, D. R. Klein, D. MacNeill, E. Navarro-Moratalla, K. L. Seyler, N. Wilson, M. A. McGuire, D. H. Cobden and D. Xiao, *et al.*, *Nat. Nanotechnol.*, 2018, **13**, 544–548.
18 Z. Wang, T. Zhang, M. Ding, B. Dong, Y. Li, M. Chen, X. Li, J. Huang, H. Wang and X. Zhao, *et al.*, *Nat. Nanotechnol.*, 2018, **13**, 554–559.
19 E. S. Morell, A. León, R. H. Miwa and P. Vargas, *2D Mater.*, 2019, **6**, 025020.
20 P. Padmanabhan, F. Buessen, R. Tutchton, K. Kwock, S. Gilinsky, M. Lee, M. McGuire, S. Singamaneni, D. Yarotski and A. Paramekanti, *et al.*, *Nat. Commun.*, 2022, **13**, 4473.
21 S. Jiang, L. Li, Z. Wang, K. F. Mak and J. Shan, *Nat. Nanotechnol.*, 2018, **13**, 549–553.
22 N. Wang, H. Tang, M. Shi, H. Zhang, W. Zhuo, D. Liu, F. Meng, L. Ma, J. Ying and L. Zou, *et al.*, *J. Am. Chem. Soc.*, 2019, **141**, 17166–17173.
23 M. Luo and Y. Shen, *JETP Lett.*, 2020, **112**, 58–63.
24 H. Iturriaga, L. M. Martinez, T. T. Mai, A. J. Biacchi, M. Augustin, A. R. Hight Walker, M. F. Sanad, S. T. Sreenivasan, Y. Liu and E. J. Santos, *et al.*, *npj 2D Mater. Appl.*, 2023, **7**, 56.
25 H. Yan, Z. Feng, S. Shang, X. Wang, Z. Hu, J. Wang, Z. Zhu, H. Wang, Z. Chen and H. Hua, *et al.*, *Nat. Nanotechnol.*, 2019, **14**, 131–136.
26 M. Zhu, Y. You, G. Xu, J. Tang, Y. Gong and F. Xu, *Intermetallics*, 2021, **131**, 107085.
27 A. León, J. González, J. Meja-López, F. C. de Lima and E. S. Morell, *2D Mater.*, 2020, **7**, 035008.
28 Z. Wu, J. Yu and S. Yuan, *Phys. Chem. Chem. Phys.*, 2019, **21**, 7750–7755.
29 T. Mukherjee, S. Chowdhury, D. Jana and L. L. Y. Voon, *J. Phys.: Condens. Matter*, 2019, **31**, 335802.

30 B. Morosin and A. Narath, *J. Chem. Phys.*, 1964, **40**, 1958–1967.
31 L. Handy and N. Gregory, *J. Am. Chem. Soc.*, 1952, **74**, 891–893.
32 M. A. McGuire, H. Dixit, V. R. Cooper and B. C. Sales, *Chem. Mater.*, 2015, **27**, 612–620.
33 H. Wang, V. Eyert and U. Schwingenschlögl, *J. Phys.: Condens. Matter*, 2011, **23**, 116003.
34 M. Wu, Z. Li, T. Cao and S. G. Louie, *Nat. Commun.*, 2019, **10**, 2371.
35 Z. Wang, I. Gutiérrez-Lezama, N. Ubrig, M. Kroner, M. Gibertini, T. Taniguchi, K. Watanabe, A. Imamoğlu, E. Giannini and A. F. Morpurgo, *Nat. Commun.*, 2018, **9**, 2516.
36 L. Pan, L. Huang, M. Zhong, X.-W. Jiang, H.-X. Deng, J. Li, J.-B. Xia and Z. Wei, *Nanoscale*, 2018, **10**, 22196–22202.
37 T. Song, X. Cai, M. W.-Y. Tu, X. Zhang, B. Huang, N. P. Wilson, K. L. Seyler, L. Zhu, T. Taniguchi and K. Watanabe, *et al.*, *Science*, 2018, **360**, 1214–1218.
38 D. R. Klein, D. MacNeill, J. L. Lado, D. Soriano, E. Navarro-Moratalla, K. Watanabe, T. Taniguchi, S. Manni, P. Canfield and J. Fernández-Rossier, *et al.*, *Science*, 2018, **360**, 1218–1222.
39 K. L. Seyler, D. Zhong, D. R. Klein, S. Gao, X. Zhang, B. Huang, E. Navarro-Moratalla, L. Yang, D. H. Cobden and M. A. McGuire, *et al.*, *Nat. Phys.*, 2018, **14**, 277–281.
40 H. H. Kim, B. Yang, S. Li, S. Jiang, C. Jin, Z. Tao, G. Nichols, F. Sfigakis, S. Zhong and C. Li, *et al.*, *Proc. Natl. Acad. Sci. U. S. A.*, 2019, **116**, 11131–11136.
41 I. Tsubokawa, *J. Phys. Soc. Jpn.*, 1960, **15**, 1664–1668.
42 W. N. Hansen, *J. Appl. Phys.*, 1959, **30**, S304–S305.
43 J. Cable, M. Wilkinson and E. Wollan, *J. Phys. Chem. Solids*, 1961, **19**, 29–34.
44 B. Kuhlow, *Phys. Status Solidi A*, 1982, **72**, 161–168.
45 F. Zheng, J. Zhao, Z. Liu, M. Li, M. Zhou, S. Zhang and P. Zhang, *Nanoscale*, 2018, **10**, 14298–14303.
46 M. A. McGuire, G. Clark, K. Santosh, W. M. Chance, G. E. Jellison Jr, V. R. Cooper, X. Xu and B. C. Sales, *Phys. Rev. Mater.*, 2017, **1**, 014001.
47 L. Webster and J.-A. Yan, *Phys. Rev. B*, 2018, **98**, 144411.
48 R. Olmos, S. Alam, P.-H. Chang, K. Gandha, I. C. Nlebedim, A. Cole, F. Tafti, R. R. Zope and S. R. Singamaneni, *J. Alloys Compd.*, 2022, **911**, 165034.
49 T. Li, S. Jiang, N. Sivadas, Z. Wang, Y. Xu, D. Weber, J. E. Goldberger, K. Watanabe, T. Taniguchi and C. J. Fennie, *et al.*, *Nat. Mater.*, 2019, **18**, 1303–1308.
50 T. Song, Z. Fei, M. Yankowitz, Z. Lin, Q. Jiang, K. Hwangbo, Q. Zhang, B. Sun, T. Taniguchi and K. Watanabe, *et al.*, *Nat. Mater.*, 2019, **18**, 1298–1302.
51 N. Richter, D. Weber, F. Martin, N. Singh, U. Schwingenschlögl, B. V. Lotsch and M. Kläui, *Phys. Rev. Mater.*, 2018, **2**, 024004.
52 S. Singamaneni, L. Martinez, J. Niklas, O. Poluektov, R. Yadav, M. Pizzochero, O. Yazyev and M. McGuire, *Appl. Phys. Lett.*, 2020, **117**, 082406.
53 J. He, S. Li, A. Bandyopadhyay and T. Frauenheim, *Nano Lett.*, 2021, **21**, 3237–3244.
54 D. Wines, K. Choudhary and F. Tavazza, *J. Phys. Chem. C*, 2023, **127**, 1176–1188.
55 F. Zhang, J. Zhang, H. Nan, D. Fang, G. Zhang, Y. Zhang, L. Liu and D. Wang, *J. Phys.: Condens. Matter*, 2022, **34**, 395901.
56 T. D. Rhone, R. Bhattarai, H. Gavras, B. Lusch, M. Salim, M. Mattheakis, D. T. Larson, Y. Krockenberger and E. Kaxiras, *Adv. Theory Simul.*, 2023, 2300019.
57 C. M. Acosta, E. Ogoshi, J. A. Souza and G. M. Dalpian, *ACS Appl. Mater. Interfaces*, 2022, **14**, 9418–9432.
58 X. Liu, D. Legut and Q. Zhang, *J. Phys. Chem. C*, 2023, **127**, 13398–13406.
59 X. Liu, D. Legut and Q. Zhang, *J. Phys. Chem. Lett.*, 2023, **14**, 7744–7750.
60 B. Yang, X. Zhang, H. Yang, X. Han and Y. Yan, *J. Phys. Chem. C*, 2018, **123**, 691–697.
61 K. Jackson and M. R. Pederson, *Phys. Rev. B: Condens. Matter Mater. Phys.*, 1990, **42**, 3276.
62 M. R. Pederson and K. A. Jackson, *Phys. Rev. B: Condens. Matter Mater. Phys.*, 1990, **41**, 7453.
63 D. Porezag and M. R. Pederson, *Phys. Rev. A: At., Mol., Opt. Phys.*, 1999, **60**, 2840.
64 J. P. Perdew, K. Burke and M. Ernzerhof, *Phys. Rev. Lett.*, 1996, **77**, 3865.
65 J. P. Perdew, K. Burke and M. Ernzerhof, *ACS Sym. Ser.*, 1996, 453.
66 T. Baruah and M. R. Pederson, *J. Chem. Theory Comput.*, 2009, **5**, 834.
67 T. Baruah, M. Olguin and R. R. Zope, *J. Chem. Phys.*, 2012, **137**, 084316.
68 M. Pederson and S. Khanna, *Phys. Rev. B: Condens. Matter Mater. Phys.*, 1999, **60**, 9566.
69 W.-B. Zhang, Q. Qu, P. Zhu and C.-H. Lam, *J. Mater. Chem. C*, 2015, **3**, 12457–12468.
70 L. Noodleman, *J. Chem. Phys.*, 1981, **74**, 5737–5743.
71 D. Torelli and T. Olsen, *2D Mater.*, 2018, **6**, 015028.
72 R. Albaridy, A. Manchon and U. Schwingenschlögl, *J. Phys.: Condens. Matter*, 2020, **32**, 355702.
73 T. Baruah and M. R. Pederson, *Chem. Phys. Lett.*, 2002, **360**, 144–148.